Inherited structural controls on normal fault architecture in the Gulf of Corinth (Greece)

Francesca Ghisetti

Department of Geology, University of Otago, Dunedin, New Zealand

Livio Vezzani

Dipartimento di Scienze della Terra, Università di Torino, Torino, Italy

Received 7 June 2004; revised 31 January 2005; accepted 13 May 2005; published 27 August 2005.

[1] In the Gulf of Corinth, E-W active normal faults and Pleistocene sedimentary basins are segmented along strike by a NNW-SSE culmination of the Hellenic thrust belt (Zarouchla culmination, ZC), which separates the Derveni-Corinth basin to the east from the Aigion basin to the west. The eastern zone is characterized by active faults with larger dimensions, cumulative throw and extension, and thicker Plio-Pleistocene clastic sequences. This distinct geometry is interpreted in terms of greater depths of penetration of the faults to the east, in agreement with earthquake depth distribution. Exhumation of deep imbricates, strong uplift, and NNW-SSE trends are consistent with ZC being the expression of upper crustal doming, consequent on NNE to NE Miocene extensional stretching, superposed onto the thrust belt. This deformed substratum, strongly oblique to the Pleistocene normal faults, acts as a geometric and mechanical barrier controlling fault segmentation to depths of ~10 km. The Corinth rift is still in its early phases of opening, and the architecture of a continental crust that is strongly heterogeneous vertically and laterally interferes with processes of growth and linkage of the evolving active normal faults plus their associated sedimentary basins.
Citation: Ghisetti, F., and L. Vezzani (2005), Inherited structural controls on normal fault architecture in the Gulf of Corinth (Greece), *Tectonics*, *24*, TC4016, doi:10.1029/2004TC001696.

1. Introduction

[2] Formation of rift basins during progressive continental extension occurs by growth of normal faults, linkage of fault segments, and accumulation of displacement on the basin-bounding faults [e.g., *Dawers and Anders*, 1995, and references therein]. Understanding fault growth requires a 3D approach, and the recognition of complex boundary conditions. Numerical and analogue models are used to focus on controversial aspects of fault growth [e.g., *Cowie et al.*, 2000], but field data and seismic profiles in different rift basins reveal large diversities in style of normal faulting (see *Corti et al.* [2003] for a review). Particularly elusive is the geometry of normal faults at depth (planar versus listric, high angle versus low angle), especially in terms of the transition from high-angle "Andersonian" normal faults in the brittle upper crust to low-angle detachments that accommodate large amounts of extensional strain in metamorphic core complexes [e.g., *Lister and Davis*, 1989].

[3] Major controlling factors of rifting in continental crust are lateral and vertical heterogeneities in lithology and rock strength. Inherited structures, mechanical barriers and weak horizons are likely to alter trajectories of fault propagation, fault growth laws, and fault kinematics.

[4] The Gulf of Corinth is an excellent area for analyzing modes and style of extensional fault growth in poly deformed, heterogeneous crust. The E-W faults that bound the rift crosscut at nearly 90° the Tertiary edifice of the Hellenic thrust belt [*Aubouin et al.*, 1970]. Extension of the thrust belt started in the Oligo-Miocene in the back arc of the Aegean trench [*Jolivet et al.*, 1999], but localized rifting in the Corinth area dates back to late Pliocene–early Pleistocene. The present crustal setting [*Tiberi et al.*, 2001] is indicative of incipient stages of rifting [*Sorel*, 2000; *Jolivet*, 2001], with fast extension rates accommodated by seismic rupturing ($M \leq 7$) of a few master faults [*Armijo et al.*, 1996]. Growth of normal faults is recorded by opening, filling and shifting of Quaternary syntectonic basins, and the geometry of the active fault sets is constrained by seismological data [e.g., *Jackson et al.*, 1982; *King et al.*, 1985; *Hatzfeld et al.*, 1996; *Hubert et al.*, 1996; *Bernard et al.*, 1997].

[5] This paper summarizes the stratigraphic and structural data acquired during our field mapping of the Aigion-Xylocastro area [*Ghisetti and Vezzani*, 2004], as part of research funded by the European Community Research Project "Corinth Rift Laboratory" [*Cornet et al.*, 2004]. Geological field data show that fault dimensions of the Pleistocene master faults, as expressed by length, cumulative throw and finite extension are larger in the eastern regions of the rift. The contrast between the eastern and western regions is also reflected by the wider extent and larger thickness of the Plio-Pleistocene syntectonic clastic sequences that infill the Derveni-Corinth basin to the east relative to the Aigion basin to the west. Geological data incorporate a long-term contrasting evolution between the

0278-7407/05/2004TC001696$12.00

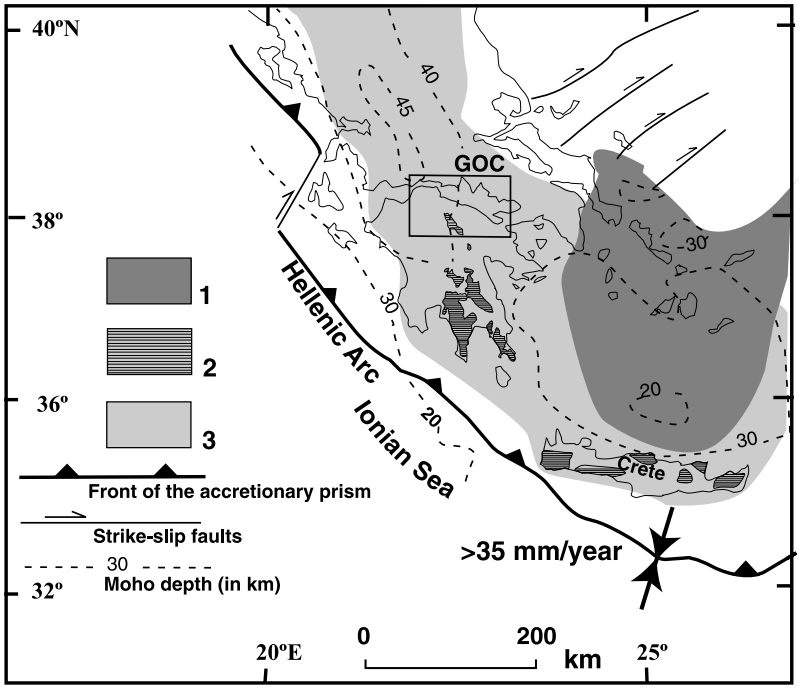

Figure 1. Location of the Gulf of Corinth (GOC) in the regional setting of the Hellenic Arc. Legend is 1, extended and exhumed lower continental crust in the Aegean Sea [from *Le Pichon et al.*, 2002]; 2, tectonic windows of the "Phyllite Series" in the Peloponnesus and Crete; and 3, domains of the Hellenic thrust belt cut by seismically active normal faults. Crustal depths are from *Makris* [1977]. The rectangle indicates the area of Figure 2.

eastern and western regions of the rift, but this difference is also reflected by present seismicity.

[6] In this paper we use the architecture of the fault network at surface to construct interpretative sections that emphasize heterogeneity and complex deformation of the upper crust, resulting from superposed phases of deformation. Geometry of normal faults at seismogenic depths is highly speculative, but segmentation of faults and sedimentary basins at surface suggests that (1) active normal faults penetrate to deeper depths in the eastern regions of the rift; (2) a geometric and mechanical barrier orthogonal to the E-W faults separates the eastern and western regions of the rift; and (3) detachment horizons on which normal faults may eventually root are discontinuous and nonplanar from east to west. Our interpretation is that the along-strike propagation of the E-W active normal faults interferes with a N-S to NNW-SSE structural culmination inherited from episodes of NNE to NE Miocene crustal stretching superposed onto the edifice of the Hellenic thrust belt.

2. Deep Structure of the Gulf of Corinth: Data and Problems

[7] In the eastern Mediterranean (Figure 1) convergence between the African and Aegean domains occurs at rates $\geq$35 mm/yr [*Le Pichon et al.*, 2002]. The accretionary prism of the Mediterranean ridge defines an arcuate subduction margin where the Ionian lithosphere plunges northward below the Hellenic trench and the continental arc (Crete and Rhodes). At the rear of the subduction margin the Aegean lithosphere has been subjected to strong extensional stretching, starting in the early Miocene [*Jolivet et al.*, 1999]. Progressive northward migration of the extensional front in the hanging wall of the subduction zone has resulted in collapse of the orogenic continental crust by distributed normal faulting, exhumation of lower continental crust in metamorphic core complexes, and extensive volcanism. Deformation is localized in discrete fault zones that accommodate the largest amount of extension. At the boundary between Peloponnesus and continental Greece (Figures 1 and 2) the Gulf of Corinth is one of the most active zones of seismic normal faulting in the Mediterranean [*Papazachos et al.*, 1998]. Extensional opening of the rift has progressed at fast rates in the last 2 Myr. Geodetic studies indicate extension rates up to 15 mm/yr [*Briole et al.*, 2000], but geological data averaged over late Quaternary times and seismic moment summation of historical earthquakes are consistent with more conservative estimates of 2–4 mm/yr [e.g., *Westaway*, 2002, and references therein]. Progressive opening of the Gulf of Corinth has been connected to extension in the back arc region of the Aegean subduction zone [*Jolivet et al.*, 1999], gravitational collapse of the orogenic edifice [*Gautier et al.*, 1999], or extension at the tip of the westward propagating North Anatolian fault [*Armijo et al.*, 2003], but crustal extension appears to be at an incipient stage [*Sorel*, 2000; *Jolivet*, 2001]. In fact, crustal tomog-

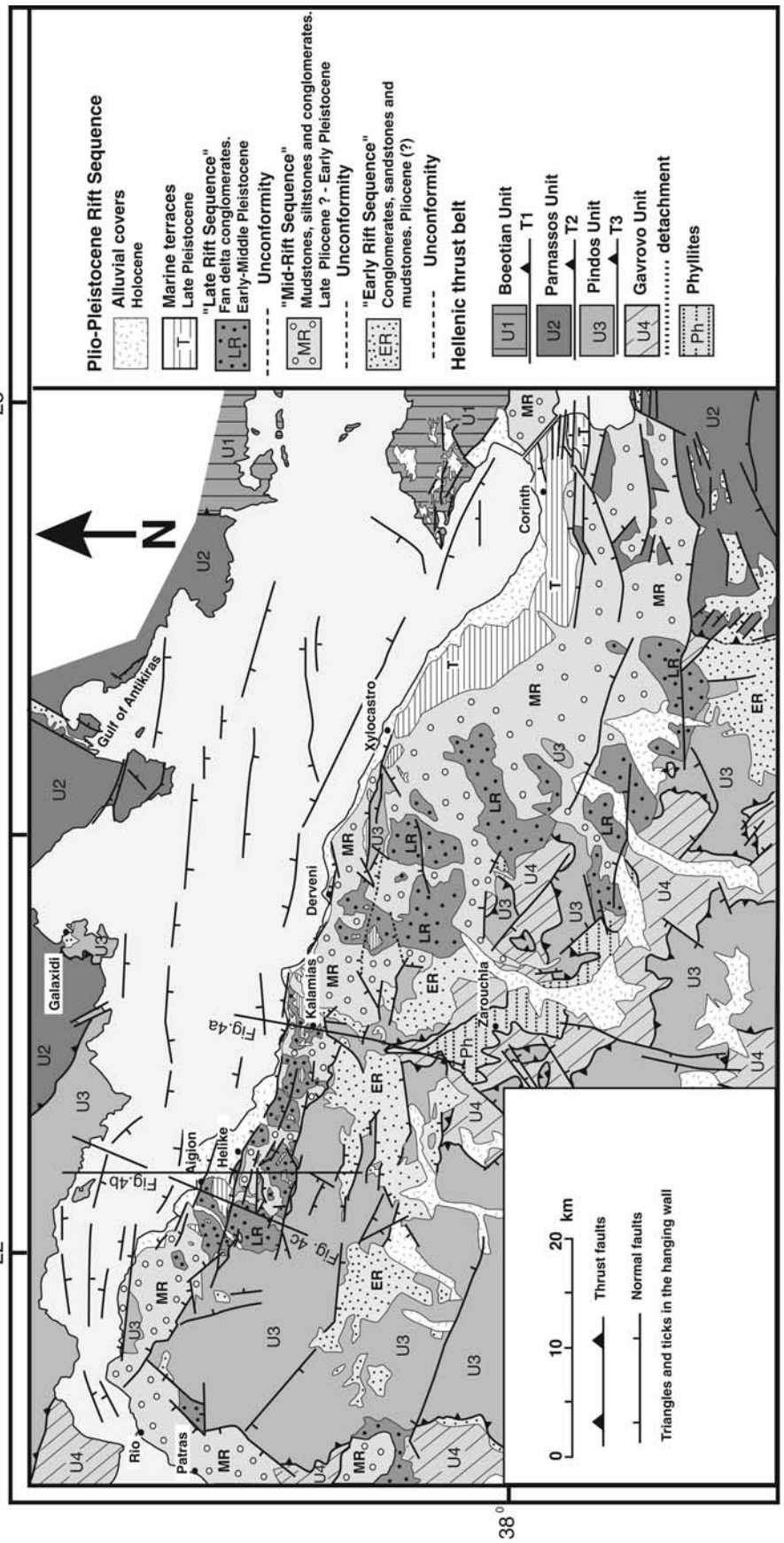

Figure 2. Simplified geological map of the Corinth rift, redrawn from a map compiled at scale 1:50,000. Sources are our new field data in the Aigion-Xylocastro region [*Ghisetti and Vezzani*, 2004] and field revisions of the map published by *Flotté* [2002].

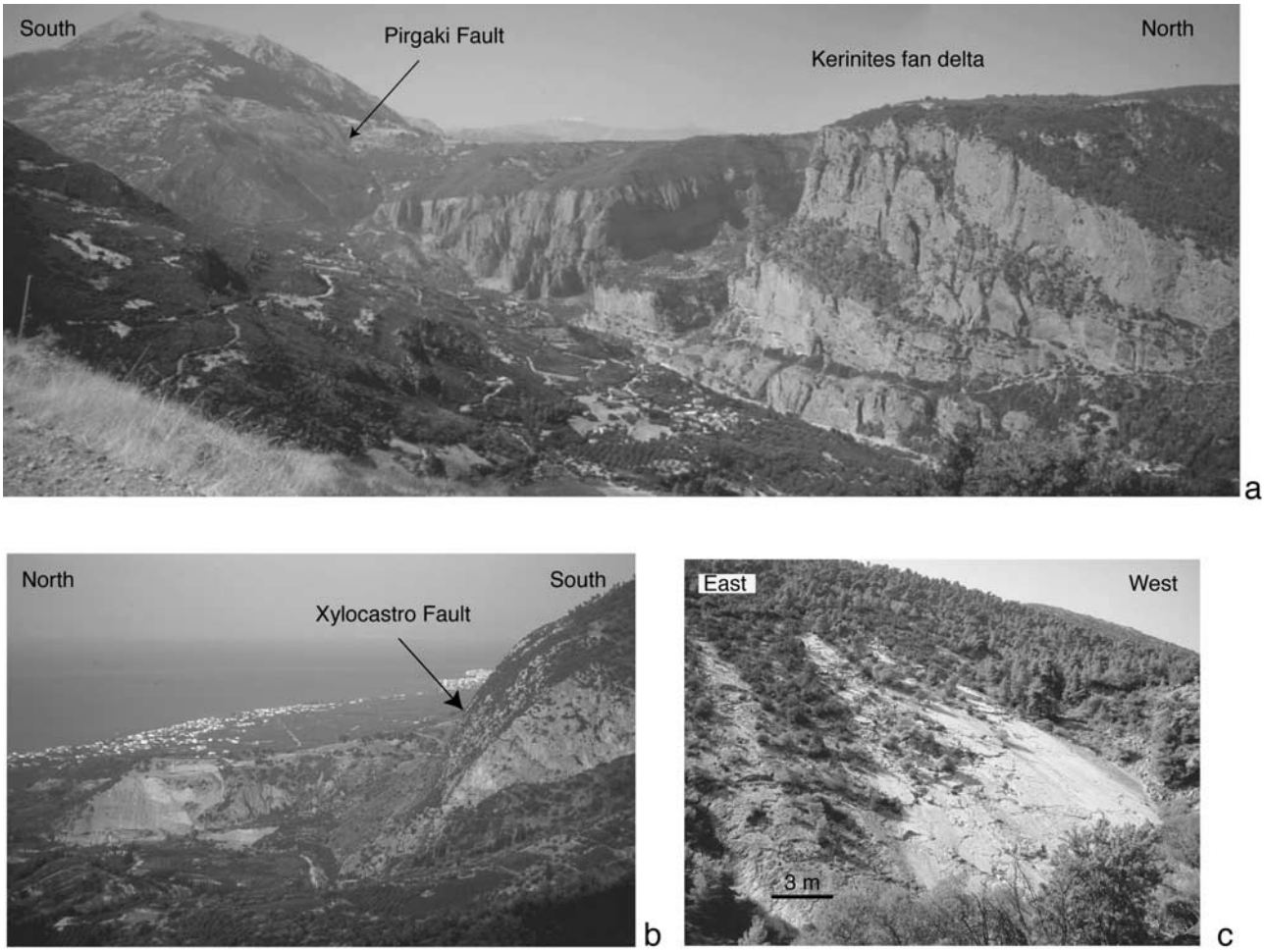

Figure 3. (a) Panorama of the Pirgaki fault on the west bank of the Kerinites river; flysch and carbonates of the Pindos Unit in the footwall. Note the thick sequence of north dipping foresets in the Kerinites fan delta and the back-tilted panel of fan delta conglomerates in the hanging wall of the Pirgaki fault. (b) Scarp of the Xylocastro fault with Pindos carbonates in the footwall and Late Rift sequence topped by marine terraces in the hanging wall. (c) Striated surface on a segment of the Xylocastro fault dipping 30–40°N. See color version of this figure at back of this issue.

raphy and inversion of gravity data [*Tiberi et al.*, 2001] show that the crust underneath the Gulf of Corinth is still more than 30 km thick (Figure 1). However, crustal thinning is detected to the southeast and to the north of the Corinth rift, giving rise to crustal-scale boudinage along NNW-SSE trends oblique to the present-day active structures and compatible with the Miocene episodes of Aegean extension [*Tiberi et al.*, 2001]. Many authors depict the Gulf of Corinth as an asymmetrical half graben with north dipping master faults on the south shore, but this view has been recently questioned by *Moretti et al.* [2003], on the basis of offshore seismic reflection profiles that reveal well-developed sets of conjugate, south dipping faults.

[8] Most fault planes are well exposed at surface (Figure 3), but the geometry of active faults at seismogenic depths remains controversial. According to *Sorel* [2000], a low-angle detachment (dip $\leq$ 20°N) that has controlled the evolution of the rift since its early inception in late Pliocene–early Pleistocene is exposed on the south shore, nearly 20–25 km south of the coastline (Khelmos detachment, Figure 4a). The Khelmos detachment is interpreted by *Sorel* [2000] as the major extensional structure that bounds the south margin of the rift and merges with the seismically active segments offshore. In this interpretation, all the high-angle faults exposed on the south shore of the rift are second-order structures to this primary detachment. There is some evidence for shallow seismic sources in the western regions of the rift, but depth of aftershocks following major earthquakes (e.g., 1981 Corinth, Ms $\leq$ 6.7; 1995 Aigion, Ms = 6.2; 1992 Galaxidi, Ms = 5.8) and distribution of microseismic events indicate an overall seismogenic thickness $\leq$15 km, with activity concentrated at depths of 6–10 km [*Rietbrok et al.*, 1996; *Bernard et al.*, 1997]. This depth cannot be easily reconciled with the

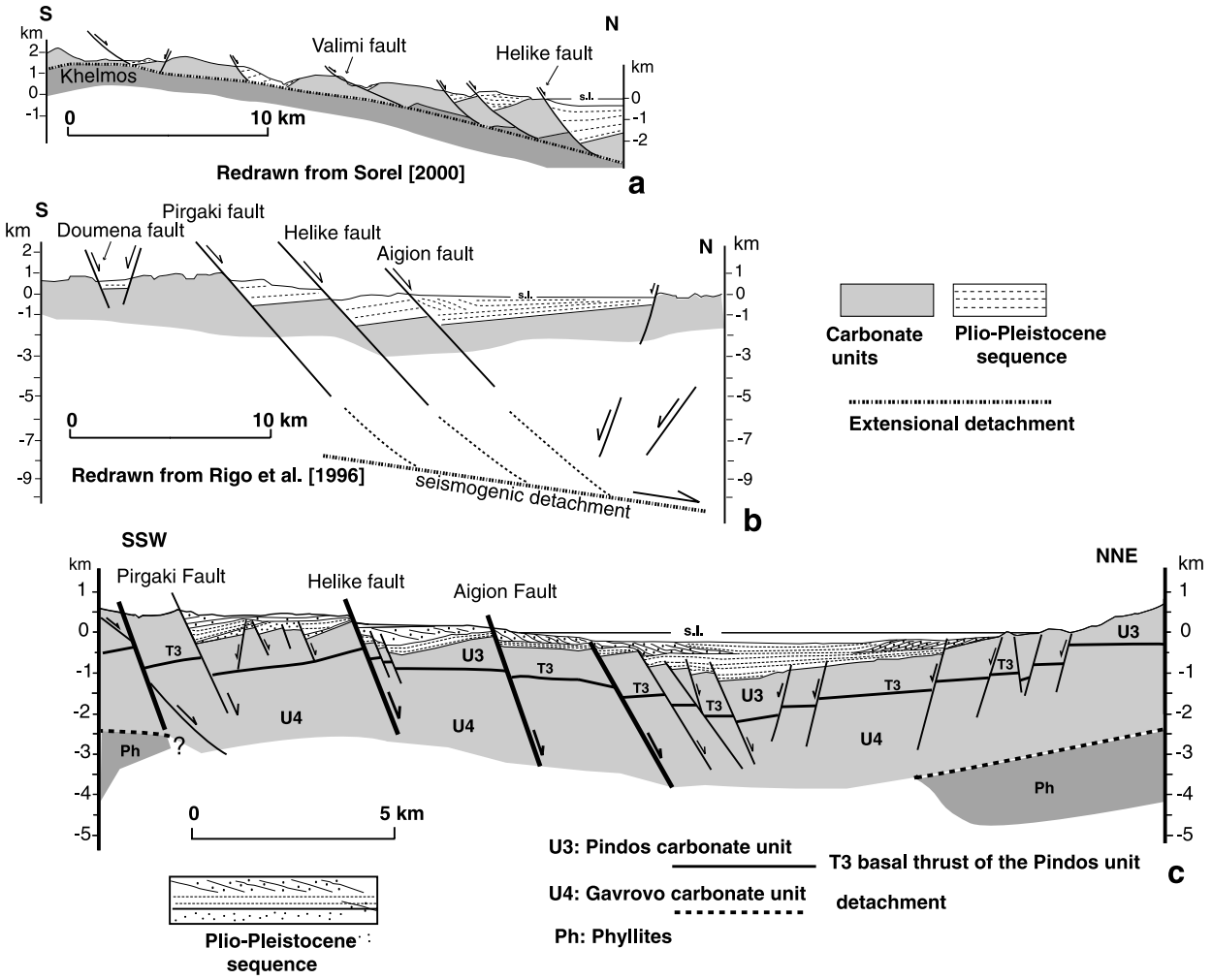

Figure 4. Interpretative cross sections of the geometry of the active normal faults in the Corinth rift. Trace of the cross sections in Figure 2. Cross section in Figure 4c is based on our field data. Note that scale is twice that of cross sections in Figures 4a and 4b. For a discussion, see text. Figure 4b is redrawn from *Rigo et al.* [1996] with permission Blackwell Publishing.

offshore projection of the Khelmos detachment (Figure 4a), as portrayed by *Sorel* [2000]. According to *Rigo et al.* [1996] the distribution of microseismicity delineates a north dipping, low-angle (15°) normal fault, located at depths of nearly 10 km underneath the north shore of the Gulf. In this interpretation, the south shore of the rift is dissected by faults with a rotated domino geometry (Figure 4b). Surface geological data constrain a steep planar geometry for almost all faults (Figure 4c and Table 1), show some evidence of southward rotated panels [*Ghisetti and Vezzani*, 2004] (Figure 4c), and indicate that the faults crosscut different thrust units of the Hellenic belt (Figures 2, 4c, and 5). However, the merging of steep faults into detachments at depths $\leq$3 km is largely unconstrained (Figure 4c), especially considering the lack of high-resolution seismic reflection images onshore. In the offshore, two NNW-SSE seismic reflection profiles in a central transect (Derveni-Itea) and in an eastern transect (Kiato-Gulf of Antikiras) [*Sachpazi et al.*, 2003] portray a different geometry of the basin bounding faults. In the central transect, high-angle, basin-bounding faults terminate at depths of 3 km into an intrabasement plane dipping 20°N. In the eastern transect, the basin-bounding faults are imaged with dips of 45°N down to depths of 5 km.

[9] In fact, a range of different data sets point to distinct deformation features between the western and eastern regions of the rift:

[10] 1. GPS measurements of present-day rates of N-S extension give average extension rates of 13–15 mm/yr in the west and 4–5 mm/yr in the east [*Briole et al.*, 2000].

[11] 2. Large earthquakes are equally distributed along the rift, but seismicity differs remarkably from west to east. In the western regions, seismicity occurs between 8 and 11 km, and recent seismic ruptures dip north at ~30°. Microseismicity levels are high [*Bernard et al.*, 1997; *Pham et al.*, 2000]. In the eastern regions seismicity is deeper

Table 1. List of Normal Faults Mapped in Figure 7[a]

Fault Name	Fault	Strike	Dip, deg	Length, km	Throw, m
Aigion	1a	289	60 NE	8.2	50–200
	1b	290	70 NE	4	100–150
	1c	285	70 NE	3	100–150
	1d	300	70 NE	3.8	150
	1e	281	70 NE	1.7	50
	1f	281	70 NE	1.9	20–50
Helike	2a	285	50 NE	16.4	300–600
Helike	2b	300	50 NE	2.3	100–150
Helike	2c	278	50–75 NE	8.2	100–300
Helike	2d	276	70 NE	1.3	100–150
Helike	2e	275	70 NE	3.3	100–150
	2f	293	70 NE	1.8	100
	2g	107	75 SW	1.1	10–30
Lakka	3a	305	70 NE	8.2	50–200
Lakka	3b	279	65 NE	4.9	50–300
	3c	278	70NE	1.5	200
	3d	277	70 NE	1.2	20
Derveni	4a	295	70 NE	1.8	100–150
Derveni	4b	286	50 NE	6.9	50–100
	4c	89	80 SE	1	20
	5	267	70 NW	2.2	20
	6	117	70 SW	1.7	200
	7	266	65 NW	3.5	50–200
	8	75	80 SE	3.6	200
	9a	321	65 NE	2	50–100
	9b	300	70 NE	2.7	50–200
	10	293	70 NE	1.5	100–150
	11	150	70 SW	1.3	100–150
	12	178	70 SW	1.6	150
Pirgaki1	13a	254	50 NW	2.4	200
Pirgaki1	13b	285	30–50 NE	4.8	500
Pirgaki2	13c	280	50–70 NE	9.3	700–1000
Pirgaki2	13d	242	70 NW	2.5	700
Pirgaki2	13e	283	70 NE	6.8	200–800
Pirgaki2	13f	300	50 NE	8.3	400–800
	13g	276	70 NE	2.5	50
	14	215	30 NW	2.2	300
	15	260	60 NW	3.5	300
	16	188	75 NW	1.8	100
	17a	125	60 SW	1.2	50
	17b	315	70 NE	2.1	50
	18a	109	70 SW	2.1	30–50
	18b	120	70 SW	1.4	30–50
	19	153	70 SW	1.6	30–50
	20	209	70 NW	3.5	30–50
	21a	96	70 SW	2.3	30
	21b	90	70 S	1.3	30
	22	105	60 SW	4.7	50–100
	23	145	70 SW	1	10
	24	218	65 NW	3	50
	25	301	70 NE	0.7	10–20
Doumena	26	281	75 NW	9.7	500–900
	27	110	70 SW	3	30
	28	214	70 NW	1.7	50
	29	36	70 SE	1.3	20
	30	259	60 NW	3.9	50–100
	31	111	70 SW	2.5	30–50
	32	281	65 NE	1.4	20
	33	242	65 NW	1	10
	34	118	60 SW	1.6	50
	35	79	60 SE	1.3	50
	36	114	70 SW	2.6	100–200
	37	90	75 S	2.2	100–200
	38	261	70 NW	2	100–200
	39	237	75 NW	3.7	200–300
	40	67	75 SE	1.7	100–200
	41	103	75 SW	6	300–500
	42	120	75 SW	1.2	20–30
	43	184	75 NW	0.8	10–20
	44	98	70 SW	3	50–150
	45	120	75 SW	1.6	20
	46	270	60 N	7	200–500
	47	260	70 NW	1.1	50
	48	311	70 NE	1.8	50
Valimi	49a	275	60 NE	5	50–300
Valimi	49b	274	70 NE	4.2	50–300
	50	341	70 NE	1.5	300–400
Vela	51	260	60 NW	8.1	500–1000
	52	88	75 SE	1.4	200
	53	250	75 NW	4.3	50–100
	54	88	75 SE	1.5	200
	55	0	65 E	1.8	200–300
	56	322	80 NE	1.6	5–10
	56	317	80 NE	1.2	5–10
	56	313	80 NE	1.9	5–10
	56	307	80 NE	0.7	5–10
	56	300	80 NE	1.2	5–10
	56	318	80 NE	0.9	5–10
	56	320	80 NE	0.6	5–10
	57	54	70 SE	1	30–50
	58	53	70 SE	1	30–50
	59	119	70 SW	1.4	30–50
	60	224	70 NW	1.7	30–50
	61	232	70 NW	1.4	150–200
Xylocastro	62	275	45–60 NE	10.7	500–2300
	63	343	80 NE	0.9	20
	64	216	70 NW	2.4	50–150
	65	277	60 NW	7.4	50–350
	66	59	70 SE	3.3	50–300
	67	85	60 SE	7.3	400–700
	68a	277	60 NE	4	100–150
	68b	253	65 NW	3.2	100–150

[a]Fault numbers indicate different faults; segments belonging to the same fault system are labeled with the same fault number and different letters. Note that not all the segments belonging to the same fault system are necessarily identified in the literature with the fault system name. Fault labeling is the same as in all figures. Fault strike is expressed with right hand rule (fault dip 90° clockwise from fault strike).Throw is calculated from offset of geological markers; along-strike variations of throw are bracketed by the extreme values.

(12–15 km) and fault planes dip 45–50° [*Jackson et al.*, 1982; *King et al.*, 1985; *Hubert et al.*, 1996]. In the central region of the rift, two recent earthquakes (Eratini 1965, Ms = 6.4; Galaxidi 1992, Ms = 5.9) were characterized by a remarkable paucity of aftershocks. *Hatzfeld et al.* [1996] attribute this anomaly to rupture of a small dimension, high strength, geometrical barrier between two of the largest faults of the south coast: the Helike fault to the west and the Xylocastro fault to the east.

[12] 3. Electrical and magnetic anisotropy [*Pham et al.*, 2000] indicate the presence of a conductive layer at depths of 10 km in the west and 20 km in the east. This conductive layer has been correlated to the low-grade metamorphic basement of the thrust belt, which may act as a detachment horizon for the largest normal faults.

[13] It is difficult to reconcile these data with only one continuous detachment that maintains an identical geometry along the strike of the rift. These factors raise the question of the role of lateral heterogeneities in controlling the

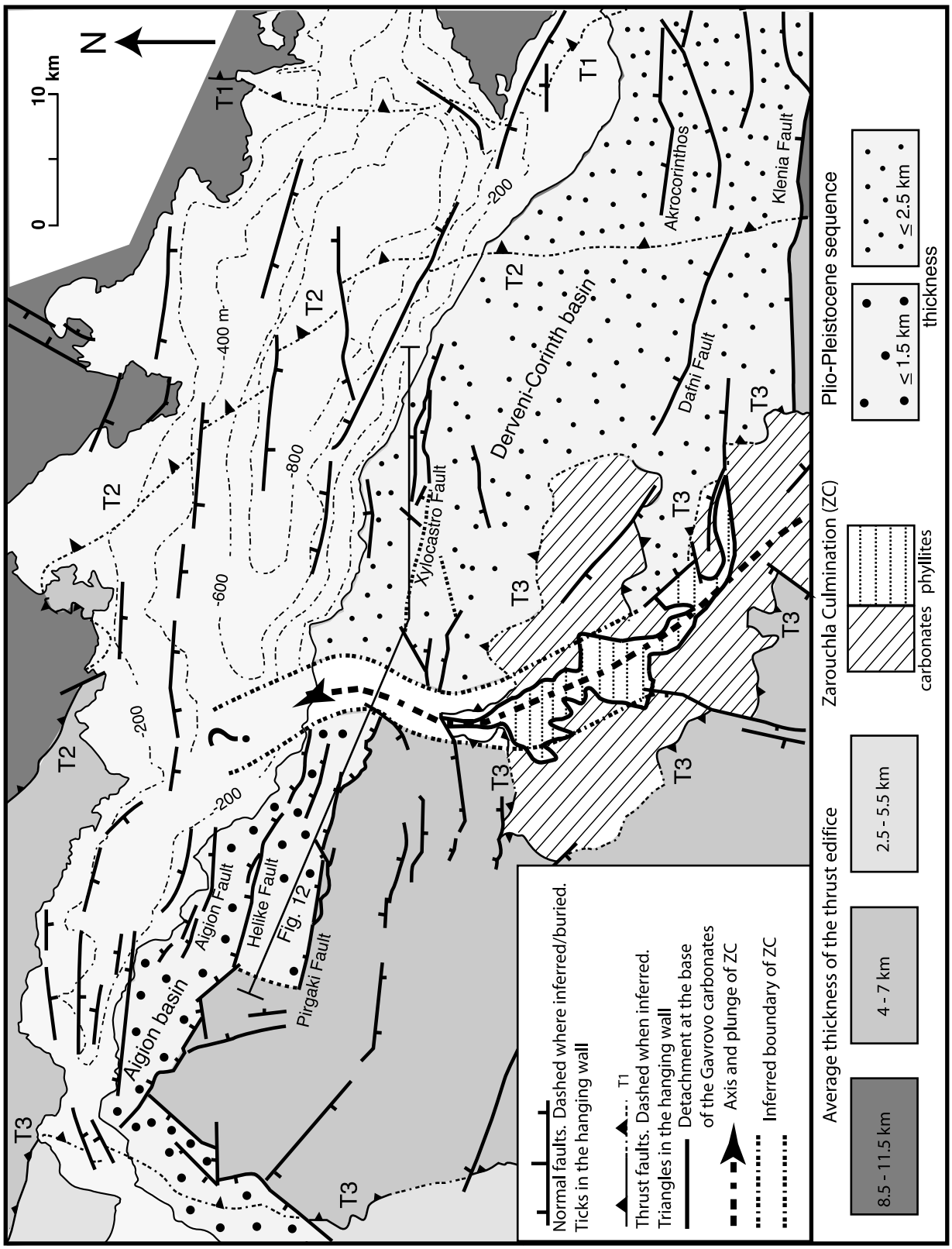
N
0
10 km
T1
T2
T3
-200
-400 m
-600
-800
Aigion basin
Aigion Fault
Helike Fault
Fig. 12
Pirgaki Fault
Xylocastro Fault
Derveni-Corinth basin
Dafni Fault
Akrocorinthos
Klenia Fault
Normal faults. Dashed where inferred/buried. Ticks in the hanging wall
Thrust faults. Dashed when inferred. Triangles in the hanging wall
Detachment at the base of the Gavrovo carbonates
Axis and plunge of ZC
Inferred boundary of ZC
Average thickness of the thrust edifice
8.5 - 11.5 km
4 - 7 km
2.5 - 5.5 km
Zarouchla Culmination (ZC)
carbonates
phyllites
Plio-Pleistocene sequence
thickness
≤ 1.5 km
≤ 2.5 km

Figure 5

architecture of normal faulting and seismically active extension.

3. Geology of the South Margin of the Gulf of Corinth

3.1. Substratum of the Rift Sequence

[14] The outcropping substratum of the Plio-Pleistocene rift basin (Figure 2) exposes a thick section of the outer Hellenic thrust edifice, with the carbonate-flysch sequence of the Boeotian, Parnassos, Pindos, and Gavrovo units, from east to west and top to bottom [*Aubouin et al.*, 1970]. Low-grade metamorphic rocks (Phyllites) are exposed in the Zarouchla Culmination (ZC) underneath the Gavrovo carbonates (Figure 2). The underlying Ionian unit and its metamorphic equivalent (Plattenkalk unit] do not crop out in the Corinth region, but their lateral extent in mainland Greece and southern Peloponnesus suggests that a >3 km thick sequence of carbonates and evaporites underlies the Phyllites in the Corinth area [*Aubouin et al.*, 1970]. A crude estimate of the average thickness that results from simple superposition of the sedimentary sequence (carbonates and flysch) of each single unit is shown in Figure 5. Thickness is larger in the east (8–11 km) and decreases westward down to 2–5 km (depending on the presence of the Ionian platform in the subsurface), in agreement with the westward vergence of the imbricates. However, larger thicknesses in the thrust belt are likely, because of folding, duplexing and eventual overthrusting of the metamorphic basement.

[15] Strong competence contrast in the imbricate stack is imparted by the tectonic interlayering of the mechanically weaker Pindos pelagic carbonates between the mechanically stronger platform carbonates of the Parnassos and Gavrovo units. Small-scale detachments are likely to be localized at the flysch-carbonate interfaces in each unit, but the most important detachment is the one that separates the Gavrovo carbonates from the underlying Phyllites in the N-S to NNW-SSE oriented ZC (Figures 2 and 5). The original geometric position of the exposed Phyllites is uncertain. If they are the Permo-Triassic sequence originally underlying the carbonates of the Gavrovo units [*Bonneau*, 1984], then the detachment is a mechanical discontinuity inherited from the contractional phases. However, according to *Bassias and Triboulet* [1994] and *Flotté* [2002], the Phyllites of ZC are part of the same belt of HP-LT metamorphic rocks, continuous from Crete to the southern Peloponnesus (''Phyllite Series'', compare Figure 1), metamorphosed to blueschist facies during Oligocene-Miocene times, and deformed by N-S synmetamorphic folds, subparallel to the stretching lineation. These rocks were exhumed as a result of forearc extension in the Miocene, and the contact with the overlying, nonmetamorphosed carbonates can be interpreted as a major extensional detachment that is partly overprinted and partly crosscut by the Plio-Pleistocene Khelmos detachment of *Sorel* [2000].

[16] The structural culmination of ZC is the most prominent feature of the substratum in the south margin of the rift. Strong components of uplift and erosion along ZC are testified by the reduced thickness of the Hellenic edifice and the deep incision of the Kratis river in the Pindos carbonates, with development of a knife-edged gorge about 40 m deep, 3 km south from the coastline (east of Kalamias in Figure 2).

3.2. Rift Sequence

[17] Since the late Pliocene, down-faulting and sea level oscillations have controlled facies and location of sedimentary basins on the north shore of Peloponnesus, with deposition of a thick ($\leq$2400 m), continental to marine clastic sequence. Today, the depocenters of the largest marine basins (Gulf of Patras, Gulf of Corinth, and Gulf of Saronicos from west to east) are controlled by E-W synsedimentary faults and are separated by ridges of the carbonate substratum (Rio Strait −65 m, Corinth isthmus, +75 m).

[18] On the south shore of the Gulf of Corinth it is possible to distinguish two basins (Aigion to the west and Derveni-Corinth to the east) bounded by E-W, north dipping faults and separated by a ridge of carbonates along ZC (Figure 5). Three clastic sequences separated by unconformities fill the basins, but facies and thickness vary considerably from east to west (Figure 6).

[19] The ''Early Rift'' sequence (coarse continental conglomerates and sandstones with interlayered mudstones, Pliocene?) fills discontinuous troughs, separated by short fault segments, dipping north and south, that are especially well developed in the western areas.

[20] The ''Mid-Rift'' sequence (late Pliocene?–early Pleistocene) shows the most important lateral variations and thickness differences from west to east (Figure 6). In the Aigion basin it consists of lacustrine mudstones (100–200 m thick) overlain by clino-stratified conglomerates (300–500 m thick). In the Derveni basin, lacustrine mudstones, sandstones and conglomerates pass upward to marine siltstones with horizons of conglomerates, with an overall thickness <1000 m; lateral closure of this sequence against ZC is supported by paleocurrent indicators of sediment dispersal from west to east, and by proximal facies adjacent to the carbonates [*Ori*, 1989].

[21] The ''Late Rift'' sequence (early middle Pleistocene) consists dominantly of clino-stratified conglomer-

Figure 5. Fault segmentation, Plio-Pleistocene basins, and thickness of the thrust belt substratum in the eastern and western regions of the Corinth rift, separated by the Zarouchla culmination (ZC) on the south margin. T1 to T3 indicate the sequence of thrust surfaces as in Figure 2. Thickness of the thrust edifice is calculated by assigning 1000 m to the Boeotian Unit, 3000 m to the Parnassos Unit, 1500 m to the Pindos Unit, 2500 m to the Gravrovo Unit, and 3000 m to the Ionian units [*Aubouin et al.*, 1970]. Bathymetry is from *Moretti et al.* [2003].

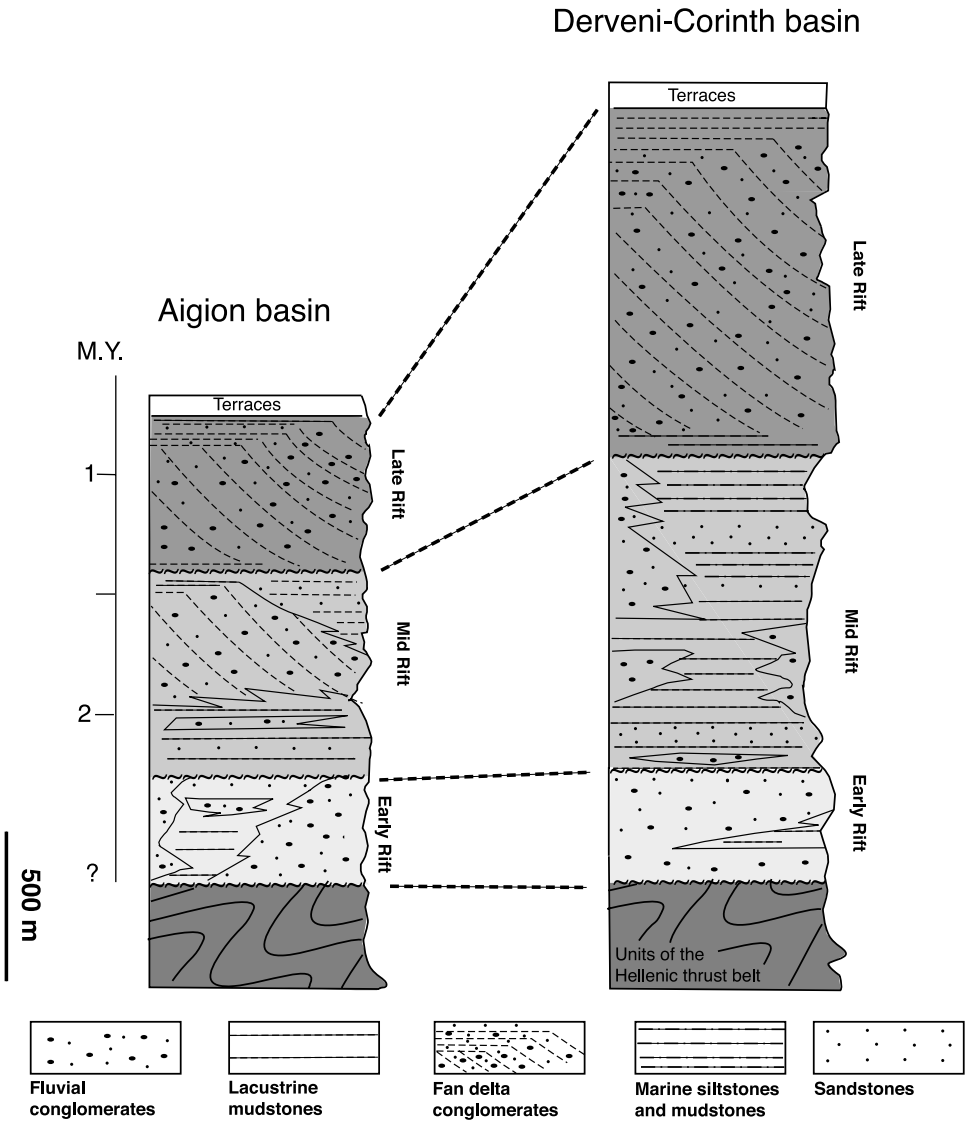

Figure 6. Synthetic stratigraphic columns of the synrift clastic sequences on the south margin of the Gulf of Corinth. Both the Aigion and Derveni-Corinth basins are characterized by lateral facies variations and thickness changes that are only schematically sketched. Scale bar is approximate.

ates (Figures 3a and 6), deposited in systems of north propagating fan deltas. Progradation of fan deltas from the rift shoulders into deeper marine basins filled with turbidites marks increasing subsidence rates during the late stages of rifting [*Ori*, 1989]. The fan deltas are 300–500 m thick in the Aigion basin and up to 1200 m thick in the Derveni-Corinth basin, where they step down from Mount Evrostini to the present coastline. Though sea level drop during Pleistocene glaciations must be taken into account [*Westaway*, 2002], down stepping of fan deltas was accommodated by sets of synsedimentary faults that shifted northward during the Pleistocene. Two such faults are the Helike and the Xylocastro faults (Figures 3b and 3c). Nowadays, the escarpment between the uplifted fan deltas and the marine Corinth basin is controlled by the Aigion fault system to the west and by sets of faults in the offshore of the Derveni-Corinth coastline (Figure 2).

4. Geometry of the Normal Faults

[22] Figure 7 and the cross sections of Figures 8 and 9 show the fault systems mapped on the southern shoulder of the Corinth rift. The majority of faults are E-W to WNW-ESE oriented and dip 60–75°N (Figures 10a and 10b and Table 1). Where measured, slickensides are dominantly dip slip, with variations in pitch between ±60–90° (compare Figure 7). Some of the longest faults are made up of segments, distinguished on the basis of variations in orientation and dip, and/or along strike variation of throw (e.g., segments 2a–2e of the Helike fault and segments 13c–13f of the Pirgaki 2 fault). Fault

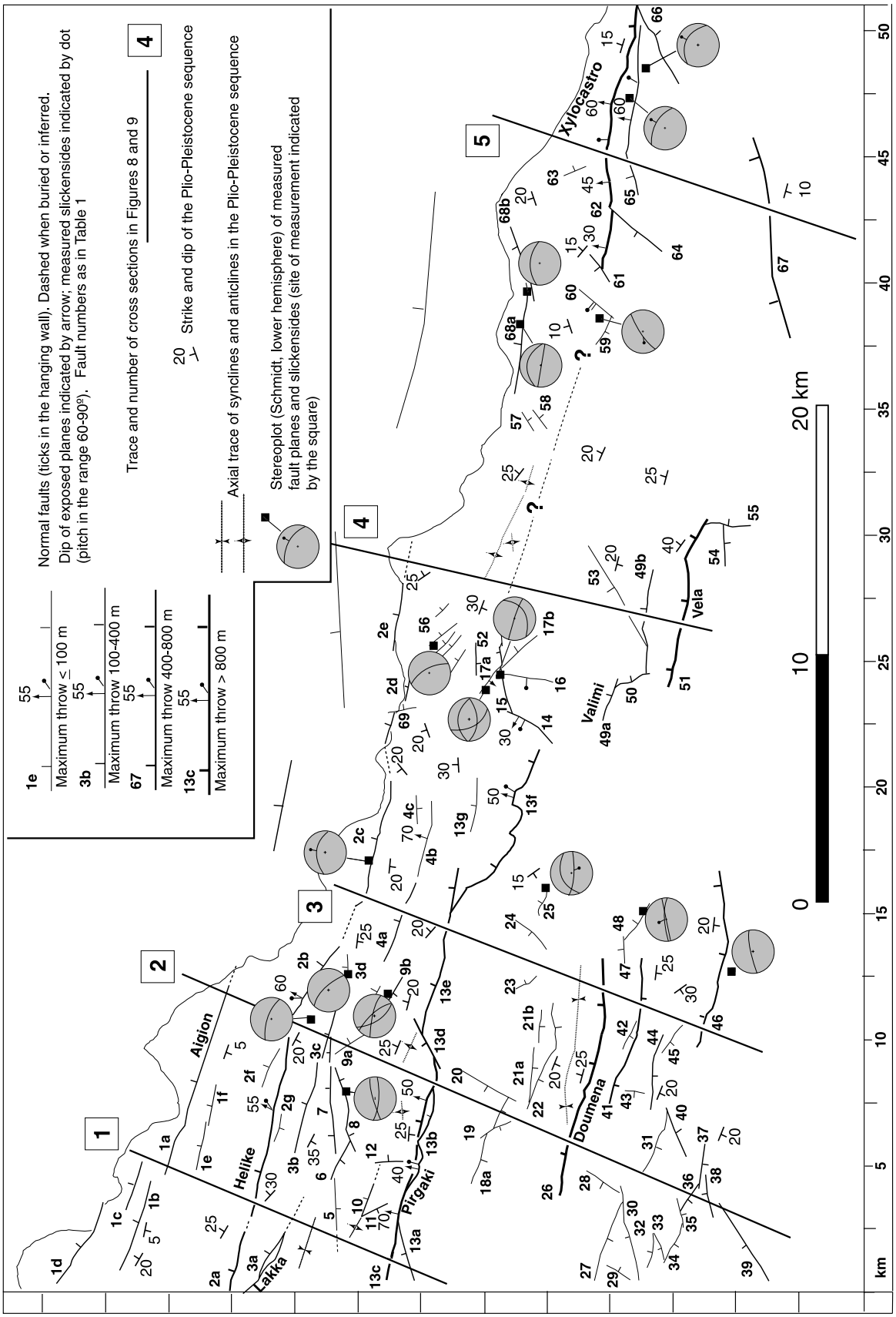
Normal faults (ticks in the hanging wall). Dashed when buried or inferred.
Dip of exposed planes indicated by arrow; measured slickensides indicated by dot (pitch in the range 60-90º). Fault numbers as in Table 1
Maximum throw < 100 m
Maximum throw 100-400 m
Maximum throw 400-800 m
Maximum throw > 800 m
Trace and number of cross sections in Figures 8 and 9
Strike and dip of the Plio-Pleistocene sequence
Axial trace of synclines and anticlines in the Plio-Pleistocene sequence
Stereoplot (Schmidt, lower hemisphere) of measured fault planes and slickensides (site of measurement indicated by the square)
Aigion
Helike
Pirgaki
Lakka
Doumena
Valimi
Vela
Xylocastro
0
10
20 km
km

Figure 7

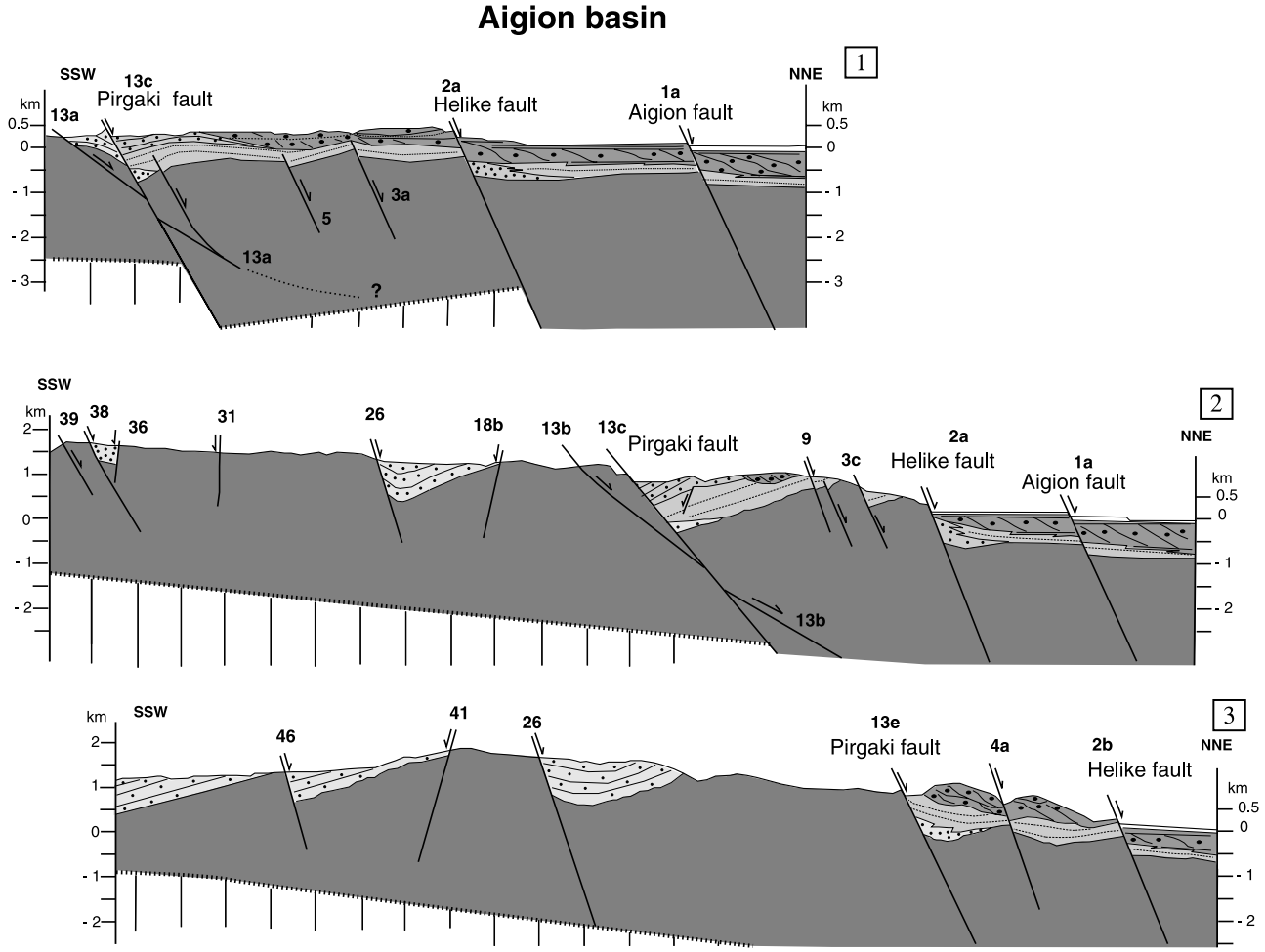

Figure 8. Cross sections in the Aigion basin. Trace is given in Figure 7. Refer to Figure 9 for legend. Fault numbers are as in Figure 7 and Table 1.

throw varies considerably, and correlation between length of individual segments and maximum throw is generally poor (Figure 10c). In part, the observed scatter may be attributed to incompleteness of the data set, as e.g., resulting from bad definition of fault segments and/or inadequate estimates of throw. Also to be taken into account is the inhomogeneity of the fault population in terms of age, with activity generally shifting northward with time [e.g., *Goldsworthy and Jackson*, 2000]. However, our data set does not show systematic variations in fault length and fault throw relatable to decreasing fault maturity from south to north. A good example is the Pirgaki fault that bounds the southern border of the "Mid Rift" sequence in the Aigion basin. The westernmost segment of the fault (13b in Figure 7 and Table 1) consists of an E-W plane dipping 30–50°N, truncated by a plane with the same orientation, dipping 70°N (cross sections 1 and 2 in Figure 8). This geometry and the folding and southward back tilting of sediments belonging to the "Mid-Rift" and "Late Rift" sequences (Figures 3a and sections 1 and 2 in Figure 8) suggest block rotation of the hanging wall panel, with formation of a new, favorably oriented fault [*Ghisetti and Vezzani*, 2004] that has the largest throw in the Aigion basin ($\leq$1 km). This setting is consistent with repeated activity of faults that maintain the same position over time. However, the complex geometry of the western Pirgaki fault is not observed in the eastern segments (13e and 13f, compare section 3 in Figure 8).

[23] Figure 11 shows the cumulative throw of the north dipping faults, measured within 2.5 $\times$ 2.5 km^2 square cells of a grid originating at the western margin of the mapped

Figure 7. Pleistocene normal faults mapped on the south shore of the Gulf of Corinth, between Aigion and Xylocastro. Cross sections 1, 2, and 3 are shown in Figure 8 and sections 4 and 5 are shown in Figure 9. The 2.5 $\times$ 2.5 km^2 square grid marked at the borders is the grid used for calculating cumulative throw and cumulative extension in Figure 11. Fault numbers are as in Table 1. See also Table 1 for length, strike, dip, and throw of each individual fault.

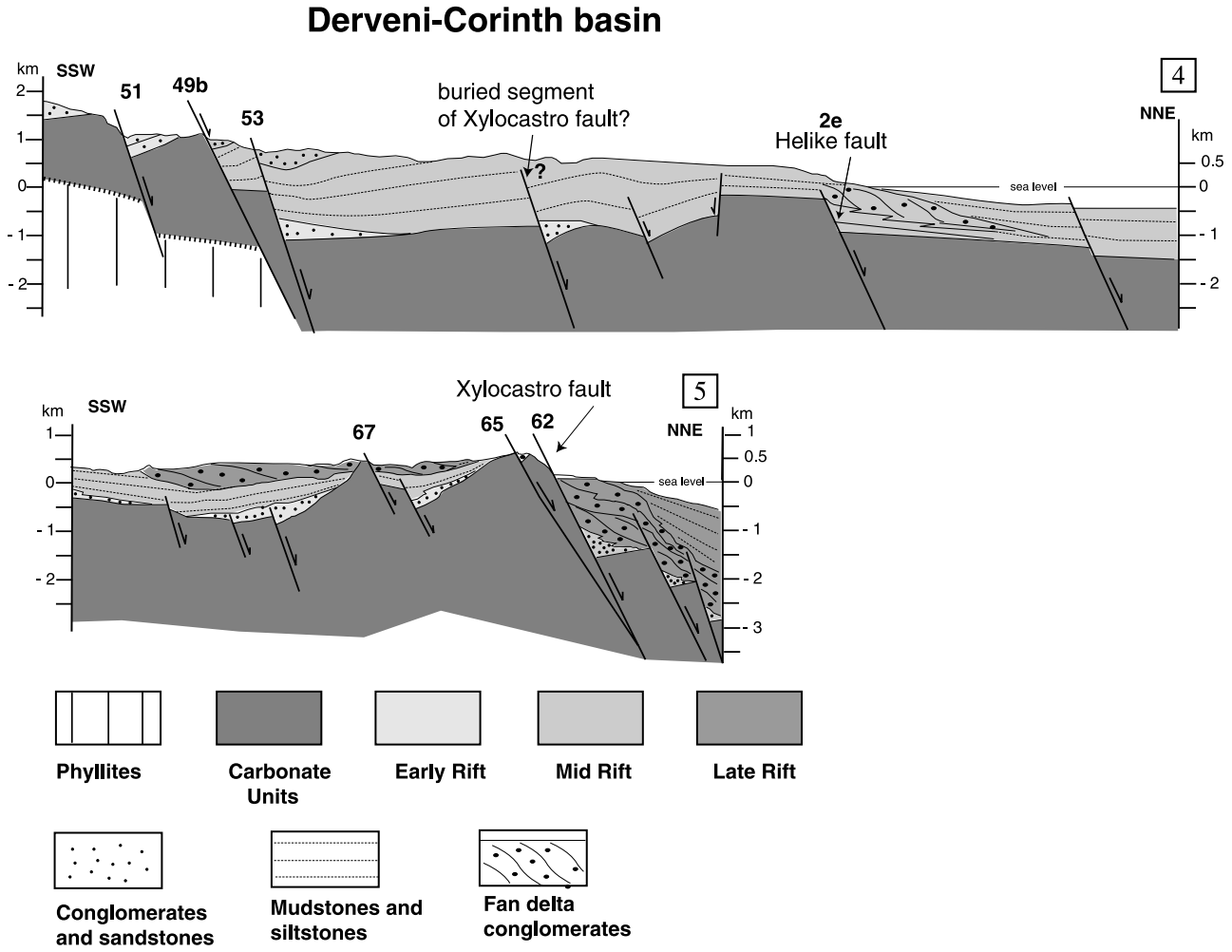

Figure 9. Cross sections in the Derveni-Corinth basin. Trace is given in Figure 7. Fault numbers are as in Figure 7 and Table 1.

area (Figure 7). The plot illustrates that: 1. the number of north dipping faults is larger in the west than in the east; 2. throw on individual faults is larger in the east; and, 3. cumulative throw diminishes toward a central area, corresponding with ZC. The same pattern is displayed by cumulative horizontal extension (ΣHext, Figure 11), calculated from the average dip (Δ) of the fault segments within each grid cell ($\Sigma Hext = \Sigma throw/\tan \Delta$). In fact, the largest faults mapped on land (Pirgaki and Helike faults in the west and Xylocastro fault in the east) cannot be traced across ZC. The along-strike continuity of the Xylocastro fault (62 in Figure 7) toward ZC is problematic. The fault is superbly exposed in the Xylocastro area (compare Figures 3b and 3c), with scarps in the striated footwall carbonates 200–300 m high. According to *Armijo et al.* [1996] throw on the fault is up to 11 km, but correlation of displaced geological units accounts only for a maximum of 2300–2500 m on the most prominent fault scarp (compare section 5 in Figure 9). It is likely that buried, subparallel faults contribute to larger cumulative throws, perhaps up to 4–6 km. The Xylocastro fault disappears in outcrop underneath the thick "Mid-Rift" sequence of the Derveni-Corinth basin. A possible westward continuation of the fault (compare section 4 in Figure 9) is inferred from an alignment of back-tilted beds and anticlinal axes in the "Mid Rift" sequence [*Ghisetti and Vezzani*, 2004], but the cumulative throw must decrease significantly westward, and there is no field evidence that a major fault aligned with the Xylocastro fault crosscuts ZC.

[24] It is possible that offshore faults crosscut ZC, but no data are available. The bathymetry of the Gulf of Corinth (Figure 5) shows a marked deepening from a shallower western portion to a >850 m deep trough in the east, consistent with the location of a deeper basin in the east, as seen for the Derveni-Corinth basin on land. A longitudinal section in the central marine trough [*Sachpazi et al.*, 2003] shows large-scale irregularities of the sediment-basement interface, with development of different depocenters, separated by culminations of the

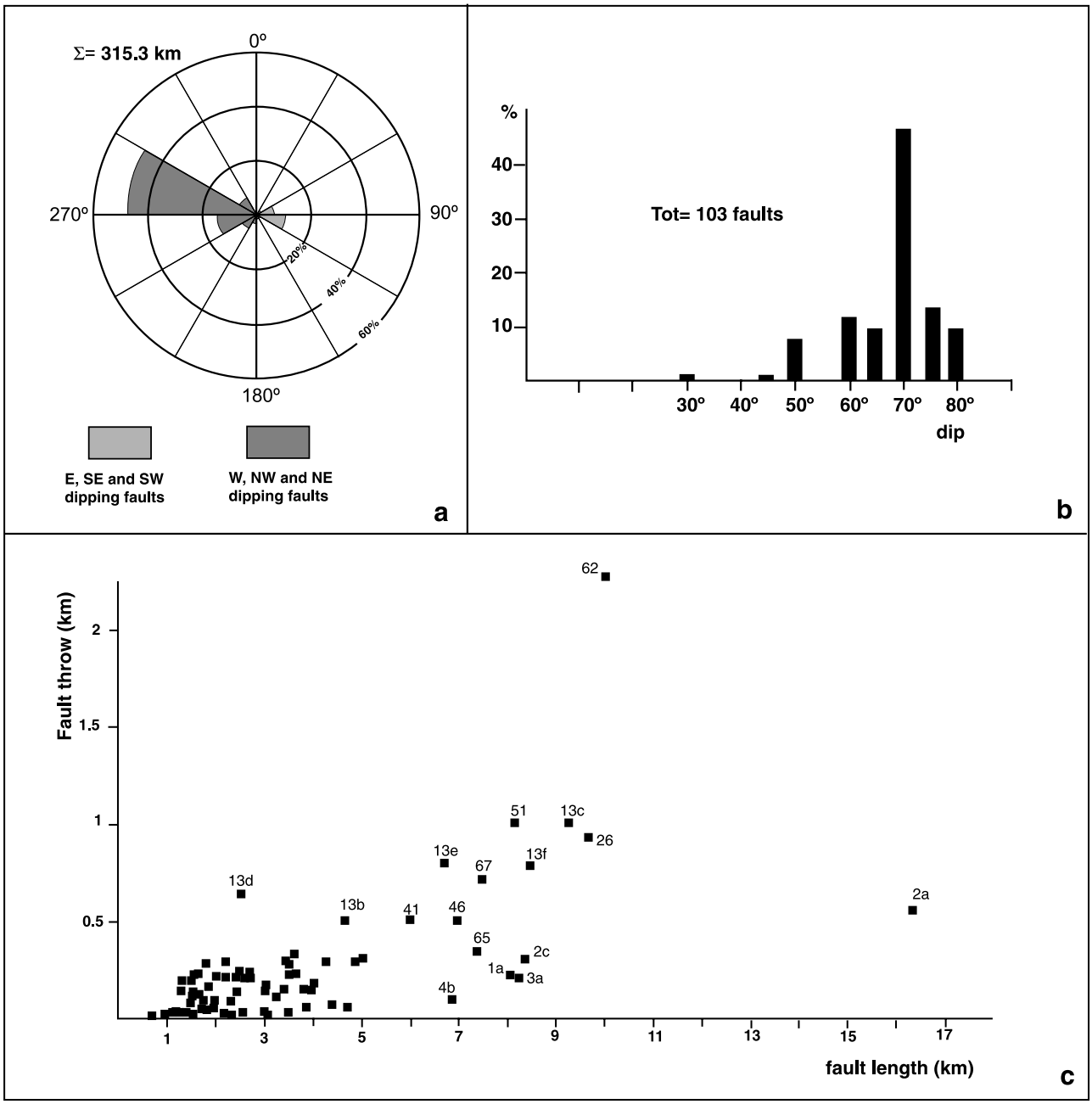

Figure 10. (a) Rose diagram of fault orientation, weighted by fault length. Orientation is expressed with right-hand rule (fault dip 90° clockwise from fault strike). (b) Histogram of fault dips as measured at surface. (c) Plot of fault throw versus length. Only the faults with the largest throw or with anomalous throw-length ratios relative to the average distribution are numbered. Fault population is the same as in Figure 7 and Table 1.

substratum, but the section does not extend as far as the projected offshore continuation of ZC.

5. Discussion

[25] The cross sections of Figures 4c, 8, and 9 illustrate the fault geometry in the south margin of the Corinth rift, as reconstructed from extrapolation of surface data down to depths <3 km.

[26] The substratum of the rift sequence is made up, from top to bottom, of the flysch-carbonate sequence of the Pindos and Gavrovo units and of the underlying Phyllites (Figure 4c), but the thrust faults and detachments that bound the different units are exposed only in ZC (Figure 2). The thrust surfaces that separate the Pindos and Gavrovo units

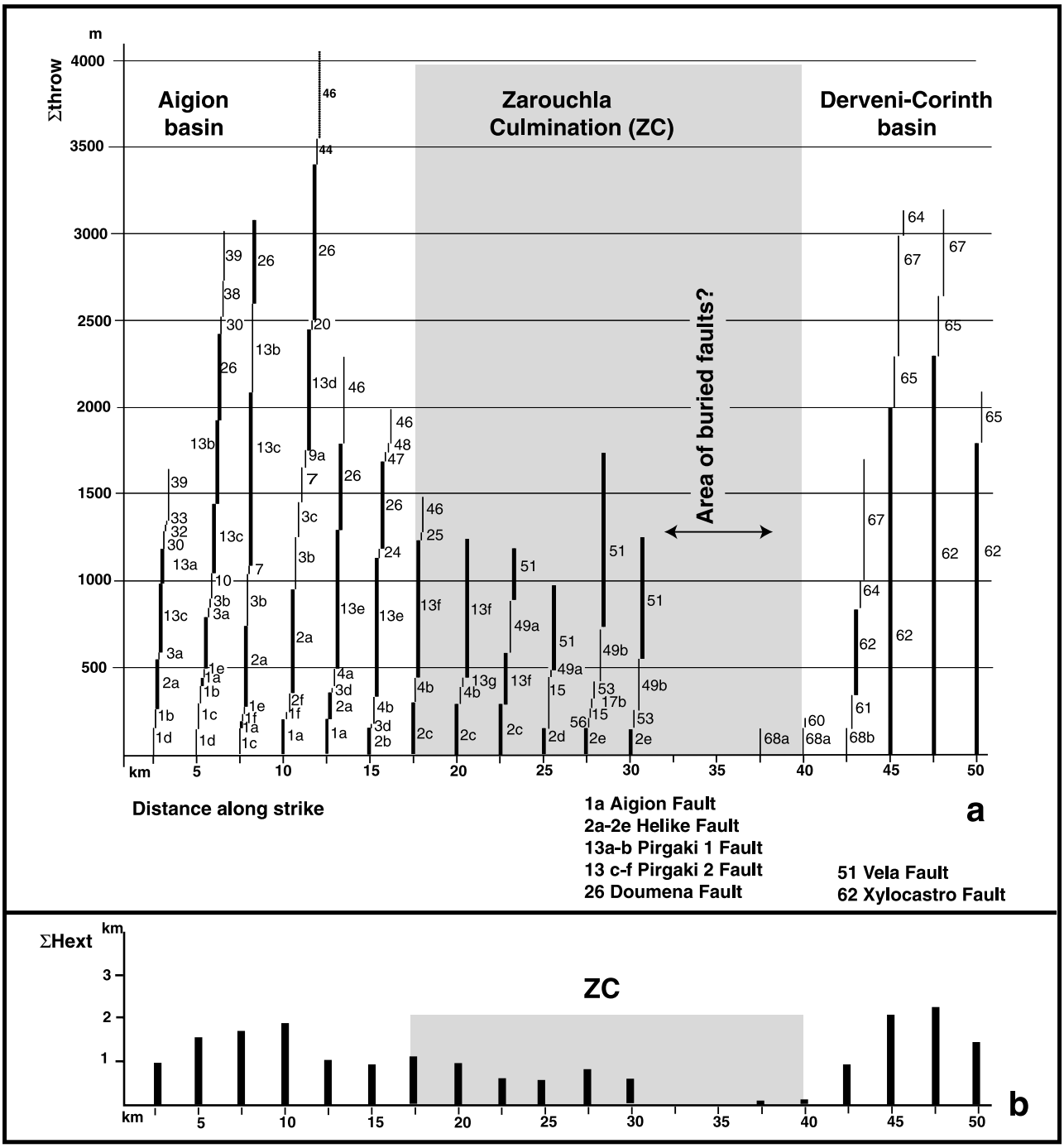

Figure 11. (a) Cumulative throw (Σthrow) of north, NE, and NW dipping faults measured in 2.5 × 2.5 km^2 square cells of a grid superposed to the map of Figure 7. Fault numbers are as in Figure 7 and Table 1. Faults with larger displacements are in bold, listed in the bottom. Throw assigned to each segment is the maximum value calibrated by offset of geological markers. (b) Cumulative horizontal extension measured within the same grid cells, as ΣHext = Σthrow/tanΔ (with Δ the average dip). The region corresponding with the Zarouchla culmination (ZC) is in grey.

are certainly cut by the normal faults (compare Figure 5), whereas the relationships between the normal faults and the Gavrovo-Phyllites detachment (GPD) are not constrained by surface data. The depth of GPD in Figures 8 and 9 is guessed on the basis of crude thickness estimations, and, as such, is prone to large and non quantified errors, depending on folding, tectonic duplications and stacking of tectonic slices within the thrust belt. The only constraint is that GPD becomes progressively shallower toward ZC, where it is in outcrop.

[27] No large fault demonstrably cuts GPD where it outcrops, and all the master faults lose displacements toward ZC (Figure 11), suggesting that GPD is not truncated in the N-S culmination. However, away from ZC, the relationships between the largest normal faults and GPD are unclear. If the detachment maintains N-S trends and remains at depths of 1–3 km in the substratum of the Aigion and Derveni-Corinth basins, it is likely to be offset by the E-W normal faults with largest dimensions and throws, as e.g., the Pirgaki, Helike (sections 1 and 2 in Figure 8) and Xylocastro faults.

[28] Extrapolation of fault dips measured at surface down to depths >3 km is also problematic. In the Aigion basin only the hanging wall panel of the western Pirgaki fault (segment 13a in Figure 7) displays back tilting of the rift sequence (Figure 3a) and roll-over folding that are consistent with domino style rotation or a listric geometry of the fault plane (compare section 1 in Figure 8). For all the other faults, there is no supporting evidence for a geometry other than planar in the top few km.

[29] Thus, though the southern margin of the Corinth rift is in an area of magnificent exposure, strong differential uplift, intense exhumation and high-rate tectonic activity, surface geology alone is unable to constrain the geometry of active faults at significant depths.

[30] However, what the surface geology does constrain is the following:

[31] 1. The different syntectonic evolution of the Aigion and Derveni-Corinth basins, separated by the carbonate ridge of ZC, and the stronger foundering of the eastern areas, as reflected by the larger thickness of the uplifted rift sequence (Figure 6), and by the deeper bathymetry in the offshore.

[32] 2. The decrease in cumulative throw and extension of the whole fault set toward ZC (Figure 11).

[33] 3. The difference in fault architecture between the Aigion basin, where many individual fault segments contribute to the overall extension ($\leq$1.9 km) and the Derveni-Corinth basin, where fewer faults with a larger throw impart a comparatively larger ($\leq$2.3 km) extension (Figure 11).

[34] If we accept the estimates of extension rates of 2–4 mm/yr averaged over a time interval of 2 Myr [*Westaway*, 2002], it is obvious that the north dipping faults exposed on land in the south shoulder of the rift contribute only a fraction (<2.3 km) of the cumulative horizontal extension (Figure 11). However, (1) some faults may be buried in the subsurface (e.g., in the Derveni-Corinth basin); (2) the most recent faults are offshore; and (3) conjugate, south dipping faults also add to the overall extension. All these contributions are not included in our data set and may explain the discrepancy. Alternatively, as proposed by *Sorel* [2000], the mapped faults are only secondary structures above a buried extensional detachment.

[35] The existence, geometry and position of a low-angle extensional detachment that controls active deformation on the Corinth rift remain controversial.

[36] The Khelmos detachment of *Sorel* [2000] coincides with the Gavrovo carbonate–Phyllites detachment in ZC but, in Sorel's interpretation (Figure 4a) the older detachment is only partially overprinted and largely dissected by a new, low-angle, Quaternary extensional fault that has an overall E-W orientation and remains buried in the substratum.

[37] When in outcrop, the detachment maintains N-S to NNW-SSE orientation. This orientation is compatible either with (1) the compressional architecture of the thrust belt or (2) the superposed Miocene extensional structures. The second alternative is plausible because (1) the metamorphic rocks in ZC are aligned with the exhumed belt of "Phyllite Series" of southern Peloponnesus and Crete, which was metamorphosed in HP-LT blueschist facies during the Oligo-Miocene [*Flotté*, 2002]; and (2) a NNW-SSE salient of the Moho topography characterizes a large region on the south of the Gulf of Corinth (compare Figure B1 of *Tiberi et al.* [2001]). These elements suggest that exhumation of the Phyllites in ZC is a late feature, superposed onto the thrust belt, and that the locus of Pleistocene rifting in Corinth was controlled by the inherited architecture of NE-SW Miocene crustal stretching.

[38] In fact, ZC appears to control the lateral segmentation between the eastern and western regions of the rift. The closure of the Aigion and Derveni-Corinth basins against ZC is indicative of the transverse carbonate ridge being emergent during Pleistocene times, possibly with strong components of uplift, in agreement with morphologic evidence for deep river incision along the Kratis river.

[39] In contrast with the work of *Sorel* [2000] we do not see much evidence for other detachments than the N-S to NNW-SSE Gavrovo carbonate-Phyllites surface exposed in ZC, which was possibly exhumed and deformed in the Miocene, long before the onset of localized rifting in the Gulf of Corinth. We also believe that the Khelmos detachment of *Sorel* [2000] is too shallow to accommodate extensional transfer of normal faults that are >10 km long, have cumulative throw up to 2–4 km (or up to 6–11 km, according to some authors) and rupture in earthquakes with M > 6 to depths of 6–15 km.

[40] We favor the interpretation portrayed in the longitudinal section of Figure 12, which emphasizes the lateral segmentation of the fault systems and related sedimentary basins, with an eastern region where (1) individual fault segments have larger dimensions and larger cumulative throw and (2) basin subsidence is greater. We relate this setting to a larger penetration of active normal faults in the east (10 km) than in the west (5–7 km) and to a progressive tapering of the E-W faults where they intersect the N-S culmination of the Gavrovo carbonate-Phyllite detachment in ZC.

[41] It is tempting to correlate a different depth of penetration of active faults to the thickness of the substratum in the Hellenic thrust belt, estimated to vary from 8–11.5 km to 4–7 km, respectively east and west of ZC (see Figure 5). If this is the case, then a feasible detachment horizon for the normal faults lies within the metamorphic basement, or at the basal interface of the Mesozoic carbonates of the Ionian unit, possibly along thick horizons of Triassic anhydrites [*Aubouin et al.*, 1970].

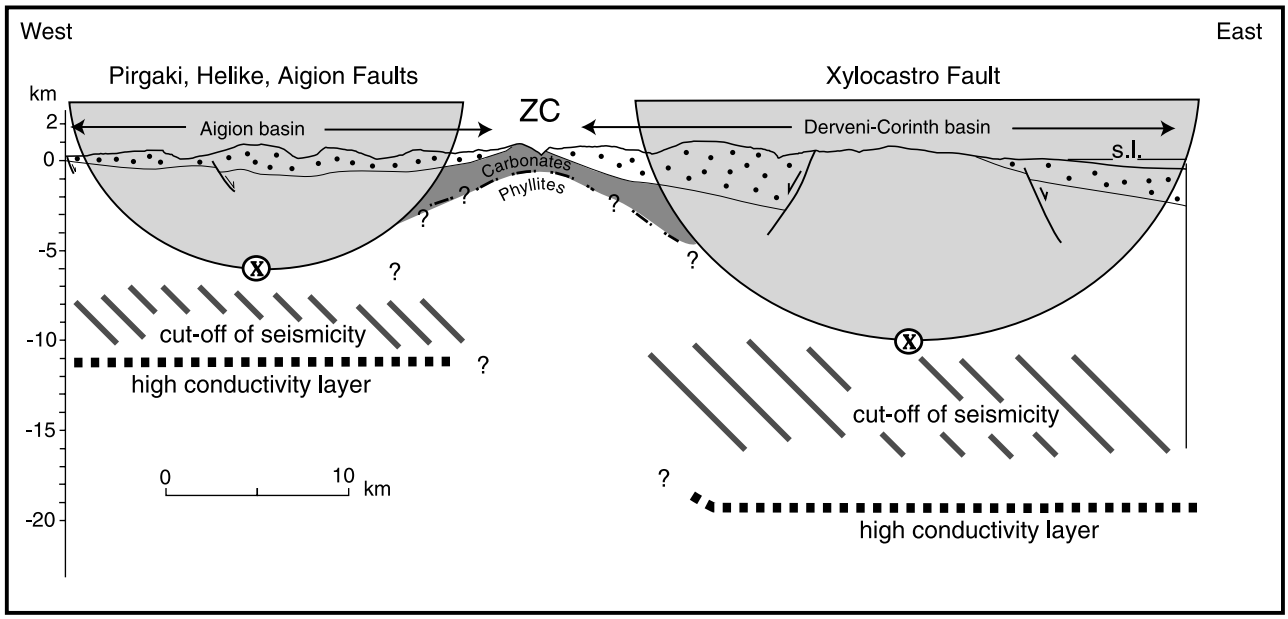

Figure 12. Longitudinal section along the south shore of the rift in the footwall of the Xylocastro and Aigion faults (trace in Figure 5). Vertical and horizontal scales are the same. ZC is the Zarouchla culmination. The grey half circles indicate the inferred lateral extension of the fault systems, as viewed from an observer in the fault footwall. The circular shape of the fault plane roughly depicts the decrease in throw toward ZC, but there is no control on a symmetrical distribution of throw relative to the fault central area. Cross marks the direction of tectonic transport, away from the observer, on fault planes dipping 50–70°N. Only the potentially seismogenic parts of the faults are illustrated. Possible ductile continuations at depth are omitted. The section incorporates geophysical data on depth of seismicity [*Hatzfeld et al.*, 2000] and the high-conductivity layer inferred from electric and magnetic anomalies [*Pham et al.*, 2000].

[42] A different depth of detachment is consistent with (1) the different depth cutoff of seismicity [*Hatzfeld et al.*, 1996; *Rigo et al.*, 1996; *Rietbrok et al.*, 1996; *Bernard et al.*, 1997] and (2) the depth of the high-conductivity layer inferred from magnetic and electrical anisotropy [*Pham et al.*, 2000]. However, the brittle faults might well continue into aseismic, localized ductile shear zones at deeper crustal levels.

[43] In Figure 12 the longitudinal continuity of the active extensional system is interrupted by a large crustal bulging that is reflected by the culmination of the detachment horizons in the upper 3–5 km. The decrease in offset of all the major faults toward ZC suggests that deformation of the deep detachment horizons has acted as a geometric and mechanical barrier to fault propagation between the western and eastern regions of the rift. The control of ZC on the lateral extent of Pleistocene sedimentary basins indicates that the barrier was not substantially broken during the phases of Pleistocene rifting, when the largest active faults were in a southern position relative to the present. The north plunge of ZC, its unclear definition offshore, and the lack of a similar structure on the north shore may indicate that the most recent offshore faults have ruptured through the barrier, as e.g., suggested by the 1965 Eratini and 1992 Galaxidi earthquakes [*Hatzfeld et al.*, 1996].

[44] Long-term faulting in response to the present N-S extension will eventually overprint and dissect the structural fabric inherited from the earlier tectonic events, but the interference of earlier structures on the growth of the Pleistocene Corinth rift is still evident in the geological record because (1) the Miocene extension has affected the structure of the upper crust, (2) the Pleistocene faults are at high angle to both the thrust belt and the Miocene extensional structures, and (3) continental rifting in Corinth is still at an incipient stage.

6. Conclusions

[45] Active fault systems and Plio-Pleistocene sedimentary basins in the Gulf of Corinth rift are segmented against a structural culmination of the thrust belt, transverse to the E-W trend of active normal faulting.

[46] The transverse structural culmination appears to have functioned as an emergent ridge separating the two sedimentary basins of Agion to the west and Derveni-Corinth to the east, and as a mechanical and geometrical barrier which interrupts the lateral propagation of a series of active normal faults (Pirgaki, Helike and Aigion Faults to the west and Xylocastro Fault to the east). The fault network in the eastern regions is characterized by larger dimensions (in fault length, cumulative throw and cumulative extension) and, accordingly, the fault-bounded sedimentary basins both inland and offshore record larger subsidence rates and sedimentary filling.

[47] We interpret these differences in terms of a larger depth of penetration of normal faults in the east (10 km) than in the west (5–7 km), eventually relatable to a greater depth of the detachment horizons at the sediment-metamorphic basement interface in the eastern, thicker regions of the Hellenic thrust belt. On the south shoulder of the rift, the longitudinal continuity of the E-W normal faults is interrupted by a NNW-SSE crustal bulging, consequent on the episodes of NE-SW Miocene extension superposed onto the thrust belt that interferes with the penetration of normal faults to seismogenic depths. Consequently, it is not likely that only one planar structure accommodates crustal extension all along the rift, in agreement with the different distribution and depth of seismicity from east to west, and with the along-strike gradient in extension rates.

[48] The Gulf of Corinth is a region where the interplay of seismically active normal faults and sedimentary basins is manifest, with the dimensions of both the faults and the basins controlled by inherited structural fabric.

[49] **Acknowledgments.** Field work was funded by the European Community Research Project "Corinth Rift Laboratory." The authors thank L. Jolivet, R. Sibson, the Editor O. Oncken, and an anonymous reviewer for criticisms and comments that greatly improved an earlier version of the manuscript.

References

Armijo, R., B. Meyer, G. C. P. King, A. Rigo, and D. Papanastassiou (1996), Quaternary evolution of the Corinth Rift and its implications for the late Cenozoic evolution of the Aegean, *Geophys. J. Int.*, *126*, 11–53.

Armijo, R., F. Flerit, G. King, and B. Meyer (2003), Linear elastic fracture mechanics explains the past and present evolution of the Aegean, *Earth Planet. Sci. Lett.*, *217*, 85–95.

Aubouin, J., et al. (1970), Contribution à la géologie des Hellènides: Le Gavrovo, le Pinde et la zone ophiolitique subpélagonienne, *Ann. Soc. Géol. Nord*, *90*, 277–306.

Bassias, Y., and C. Triboulet (1994), Tectono-metamorphic evolution of blueschist formations in the Peloponnesus (Parnon and Taygetos Massifs, Greece): A model of nappe stacking during Tertiary orogenesis, *J. Geol.*, *102*, 697–708.

Bernard, P., et al. (1997), The Ms = 6.2, June 15, 1995 Aigion earthquake (Greece): evidence for low angle normal faulting in the Corinth rift, *J. Seismol.*, *1*, 131–150.

Bonneau, M. (1984), Correlation of the Hellenide nappes in the south-east Aegean and their tectonic reconstruction, in *The Geological Evolution of the Eastern Mediterranean*, edited by J. E. Dixon and H. F. Robertson, *Geol. Soc. Spec. Publ.*, *17*, 517–527.

Briole, P., A. Rigo, H. Lyon Caen, J. C. Ruegg, K. Papazissi, C. Mitsakaki, A. Balodimou, G. Veis, D. Hatzfeld, and A. Deschamps (2000), Active deformation of the Corinth rift, Greece: Results from repeated Global Positioning System surveys between 1990 and 1995, *J. Geophys. Res.*, *105*, 25,605–25,625.

Cornet, F. H., I. Moretti, and P. Bernard (2004), Le laboratoire du rift de Corinthe, *C.R. Geoscience*, *336*, 485 pp.

Corti, G., M. Bonini, S. Conticelli, F. Innocenti, P. Manetti, and D. Sokoutis (2003), Analogue modelling of continental extension: A review focused on the relations between the patterns of deformation and the presence of magma, *Earth Sci. Rev.*, *63*, 169–247.

Cowie, P. A., S. Gupta, and N. H. Dawers (2000), Implications of fault array evolution for synrift depocentre development: Insights from a numerical fault growth model, *Basin Res.*, *12*, 241–261.

Dawers, N. H., and M. H. Anders (1995), Displacement-length scaling and fault linkage, *J. Struct. Geol.*, *17*, 607–614.

Flotté, N. (2002), Caracterisation structurale et cinematique d'un rift sur detachment: Le rift de Corinthe-Patras, Grèce, thèse de Doctorat, 197 pp., Univ. Paris XI, Paris.

Gautier, P., J. P. Brun, R. Moriceau, D. Sokoutis, J. Martinod, and L. Jolivet (1999), Timing, kinematics and cause of Aegean extension: A scenario based on a comparison with simple analogue experiments, *Tectonophysics*, *315*, 31–72.

Ghisetti, F., and L. Vezzani (2004), Plio-Pleistocene sedimentation and fault segmentation in the Gulf of Corinth (Greece) controlled by inherited structural fabric, *C.R. Geoscience*, *336*, 243–249.

Goldsworthy, M., and J. A. Jackson (2000), Active normal fault evolution in Greece revealed by geomorphology and drainage patterns, *J. Geol. Soc. London*, *157*, 967–981.

Hatzfeld, D., et al. (1996), The Galaxidi earthquake of 18 November 1992: A possible asperity within the normal fault system of the Gulf of Corinth (Greece), *Seismol. Soc. Am. Bull.*, *86*, 1987–1991.

Hatzfeld, D., V. Karakostas, M. Ziazia, I. Kassaras, E. Papadimitriou, K. Makropoulos, N. Voulgaris, and C. Papaioannou (2000), Microseismicity and faulting geometry in the Gulf of Corinth (Greece), *Geophys. J. Int.*, *141*, 438–456.

Hubert, A., G. King, R. Armijo, B. Meyer, and D. Papanastasiou (1996), Fault re-activation, stress interaction and rupture propagation of the 1981 Corinth earthquake sequence, *Earth Planet. Sci. Lett.*, *144*, 611–613.

Jackson, J. A., J. Gagnepain, G. Houseman, G. C. P. King, P. Papadimitriou, C. Soufleris, and J. Virieux (1982), Seismicity, normal faulting, and the geomorphological development of the Gulf of Corinth (Greece): The Corinth earthquakes of February and March 1981, *Earth Planet. Sci. Lett.*, *57*, 377–397.

Jolivet, L. (2001), A comparison of geodetic and finite strain pattern in the Aegean: Geodynamic implications, *Earth Planet. Sci. Lett.*, *187*, 95–104.

Jolivet, L., C. Faccenna, N. D'Agostino, M. Fournier, and D. Worrall (1999), The kinematics of back-arc basins, examples from the Tyrrhenian, Aegean and Japan Seas, in *Continental Tectonics*, edited by C. Mac Niocaill and P. D. Ryan, *Geol. Soc. Spec. Publ.*, *164*, 21–53.

King, G. C. P., Z. X. Ouyang, P. Papadimitriou, A. Deschamps, J. Gagnepain, G. Houseman, J. A. Jackson, C. Soufleris, and J. Virieux (1985), The evolution of the Gulf of Corinth (Greece): An aftershock study of the 1981 earthquakes, *Geophys. J. R. Astron. Soc.*, *80*, 677–683.

Le Pichon, X., S. J. Lallemant, N. Chamot-Rooke, D. Lemeur, and G. Pascal (2002), The Mediterranean Ridge backstop and the Hellenic nappes, *Mar. Geol.*, *186*, 111–125.

Lister, G. S., and G. A. Davis (1989), The origin of metamorphic core complexes and detachment faults formed during Tertiary continental extension in the northern Colorado river region, U.S.A., *J. Struct. Geol.*, *11*, 65–94.

Makris, J. (1977), Geophysical Investigation of the Hellenides, *Hamburger Geophysikalische Einzelschriften*, *34*, 124 pp., Geophys. Inst., Univ. Hamburg, Hamburg, Germany.

Moretti, I., D. Sakellariou, V. Lykousis, and L. Micarelli (2003), The Gulf of Corinth: An active half graben?, *J. Geodyn.*, *36*, 323–340.

Ori, G. G. (1989), Geologic history of the extensional basin of the Gulf of Corinth (?Miocene-Pleistocene), Greece, *Geology*, *17*, 918–921.

Papazachos, B. C., E. Papadimitriou, A. A. Kiratzi, C. B. Papazachos, and E. K. Louvari (1998), Fault plane solutions in the Aegean Sea and the surrounding area and their tectonic implication, *Boll. Geof. Teor. Appl.*, *39*, 199–218.

Pham, V. N., P. Bernard, D. Boyer, G. Chouliaras, I. L. Le Mouel, and G. N. Stavrakakis (2000), Electrical conductivity and crustal structure beneath the central Hellenides around the Gulf of Corinth (Greece) and their relationship with the seismotectonics, *Geophys. J. Int.*, *142*, 948–969.

Rietbrock, A., C. Tiberi, F. Scherbaum, and H. Lyon Caen (1996), Seismic slip on a low angle normal fault in the Gulf of Corinth: Evidence from high-resolution cluster analysis of microearthquakes, *Geophys. Res. Lett.*, *23*, 1817–1820.

Rigo, A., H. Lyon-Caen, R. Armijo, A. Deschamps, D. Hatzfeld, K. Makropoulos, P. Papadimitriou, and I. Kassaras (1996), A microseismic study in the western part of the Gulf of Corinth (Greece): Implications for large-scale normal faulting mechanisms, *Geophys. J. Int.*, *126*, 663–688.

Sachpazi, M., C. Clément, M. Laigle, A. Hirn, and N. Roussos (2003), Rift structure, evolution, and earthquakes in the Gulf of Corinth, from reflection seismic images, *Earth Planet. Sci. Lett.*, *216*, 243–257.

Sorel, D. (2000), A Pleistocene and still-active detachment fault and the origin of the Corinth-Patras rift, Greece, *Geology*, *28*, 83–86.

Tiberi, C., M. Diament, H. Lyon-Caen, and T. King (2001), Moho topography beneath the Corinth Rift area (Greece) from inversion of gravity data, *Geophys. J. Int.*, *145*, 797–808.

Westaway, R. (2002), The Quaternary evolution of the Gulf of Corinth, central Greece: Coupling between surface processes and flow in the lower continental crust, *Tectonophysics*, *348*, 269–318.

F. Ghisetti, Department of Geology, University of Otago, P.O. Box 56, 9001 Dunedin, New Zealand. (francesca.ghisetti@stonebow.otago.ac.nz)

L. Vezzani, Dipartimento di Scienze della Terra, Università di Torino, Via Accademia delle Scienze 5, I-10123 Torino, Italy.

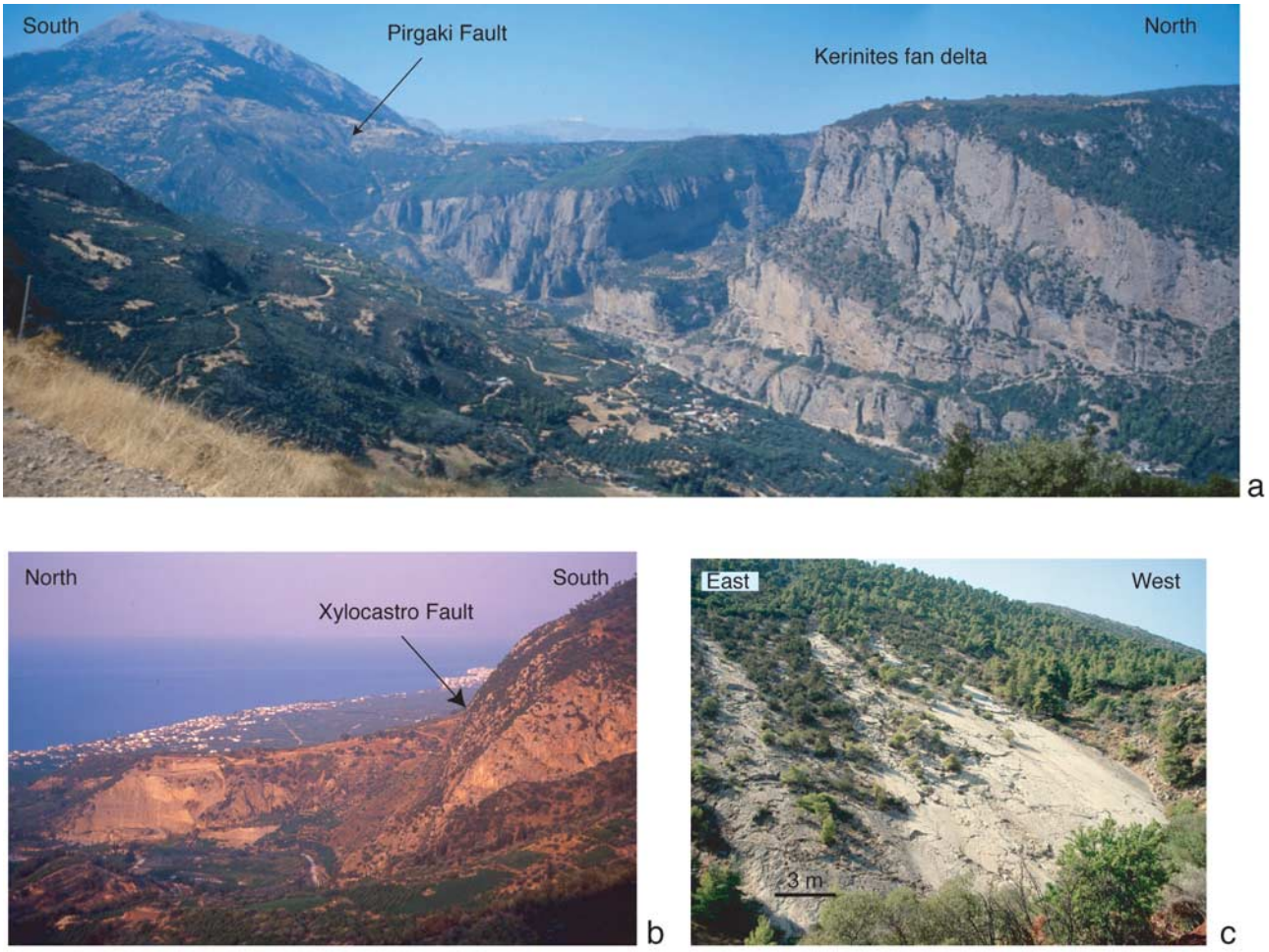

Figure 3. (a) Panorama of the Pirgaki fault on the west bank of the Kerinites river; flysch and carbonates of the Pindos Unit in the footwall. Note the thick sequence of north dipping foresets in the Kerinites fan delta and the back-tilted panel of fan delta conglomerates in the hanging wall of the Pirgaki fault. (b) Scarp of the Xylocastro fault with Pindos carbonates in the footwall and Late Rift sequence topped by marine terraces in the hanging wall. (c) Striated surface on a segment of the Xylocastro fault dipping 30–40°N.